Biogeosciences
Discussions

Open Access

Biophysical controls on net ecosystem CO$_2$ exchange over a semiarid shrubland in northwest China

X. Jia[1], T. S. Zha[2], B. Wu[3], Y. Q. Zhang[1], J. N. Gong[2], S. G. Qin[3], G. P. Chen[1], S. Kellomäki[2], and H. Peltola[3]

[1]Yanchi Research Station, School of Soil and Water Conservation, Beijing Forestry University, Beijing 100083, China
[2]School of Forest Sciences, University of Eastern Finland, P.O. Box 111, 80101 Joensuu, Finland
[3]Institute of Forest Sciences, Bailongjiang Forestry Management Bureau, Wudu, Gansu 746010, China

Correspondence to: T. S. Zha (tianshanzha@bjfu.edu.cn)

BGD

11, 5089–5122, 2014

Biophysical controls on NEE over a semiarid shrubland

X. Jia et al.

Title Page

Abstract | Introduction

Conclusions | References

Tables | Figures

◄ | ►

◄ | ►

Back | Close

Full Screen / Esc

Printer-friendly Version

Interactive Discussion

Abstract

The carbon (C) cycling in semiarid and arid areas remains largely unexplored, despite the wide distribution of drylands globally. Rehabilitation practices have been carried out in many desertified areas, but information on the C sequestration potential of recovering vegetation is still largely lacking. Using the eddy-covariance technique, we measured the net ecosystem CO_2 exchange (NEE) over a recovering shrub ecosystem in northwest China throughout 2012 in order to (1) quantify NEE and its components, (2) examine the dependence of C fluxes on biophysical factors at multiple timescales. The annual budget showed a gross ecosystem productivity (GEP) of $456 \pm 8\,\mathrm{g\,C\,m^{-2}\,yr^{-1}}$ and an ecosystem respiration (R_e) of $379 \pm 3\,\mathrm{g\,C\,m^{-2}\,yr^{-1}}$, resulting in a net C sink of $77 \pm 7\,\mathrm{g\,C\,m^{-2}\,yr^{-1}}$. The maximum daily NEE, GEP and R_e were -4.7, 6.8 and $3.3\,\mathrm{g\,C\,m^{-2}\,day^{-1}}$, respectively. Both the maximum C assimilation rate (i.e., at optimum light intensity) and the quantum yield varied strongly over the growing season, being higher in summer and lower in spring and autumn. At the half-hourly scale, water stress exerted a major control over daytime NEE, and interacted with heat stress and photoinhibition in constraining C fixation by the vegetation. Low soil moisture also reduced the temperature sensitivity of R_e (Q_{10}). At the synoptic scale, rain events triggered immediate pulses of C release from the ecosystem, followed by peaks of CO_2 uptake 1–2 days later. Over the entire growing season, leaf area index accounted for 45 and 65 % of the seasonal variation in NEE and GEP, respectively. There was a linear dependence of daily R_e on GEP, with a slope of 0.34. These results highlight the role of abiotic stresses and their alleviation in regulating C cycling in the face of an increasing frequency and intensity of extreme climatic events.

1 Introduction

Drylands (semiarid and arid areas) cover over 40 % of the Earth's land surface, and are rapidly expanding as a result of climate change and human activities (Asner et al.,

Full Screen / Esc

Printer-friendly Version

Interactive Discussion

Biophysical controls on NEE over a semiarid shrubland

X. Jia et al.

Full Screen / Esc

Printer-friendly Version

Interactive Discussion

2003). Although dryland ecosystems are characterized by low precipitation (PPT), soil fertility and productivity, they are important to the global carbon (C) budget as they account for approximately 20 % of total terrestrial net primary productivity (Whittaker, 1975) and 15 % of total soil organic carbon (Lal, 2004). The C cycling in desert ecosys-
5 tems is particularly sensitive to climate and land-use changes, and may feed back to the climate system (Li et al., 2005). In order to accurately predict global C cycling under changing climate, it is necessary to understand how CO_2 exchange in dry areas responds to variations in climatic conditions (Gao et al., 2012). Currently, the C dynamics of desert shrub ecosystems and their responses to environmental factors are
10 less-well-known compared to those of forests and grasslands (Gao et al., 2012).

Whether a dryland ecosystem is a net sink or source of CO_2 is affected by the way it responds to climatic variability (Liu et al., 2012). In semiarid and arid ecosystems, moisture related factors such as PPT, soil water content (SWC) and vapor pressure deficit (VPD) usually exert strong influences on diurnal, seasonal and interannual vari-
15 ations in the net ecosystem CO_2 exchange (NEE) (Fu et al., 2006; Gao et al., 2012). Water deficit may depress gross ecosystem productivity (GEP) by limiting plant physiological processes (e.g., stomatal closure) and altering plant phenology (e.g., delayed leaf emergence) and canopy structure (e.g., reduced leaf area index, LAI) (Zhou et al., 2013). Low water availability may also limit ecosystem respiration (R_e) by reducing root
20 activity, suppressing microbial decomposition of organic matters and restricting the diffusion of extra-cellular enzymes and C substrates in the soil (Wang et al., 2014). Moreover, the effects of water availability on GEP and R_e depend not only on the sensitivity of related biotic processes and the magnitude of water stress, but also on the temporal pattern of water supply. For example, NEE in dryland ecosystems showed complex and
25 inconsistent responses to rainfall events (Liu et al., 2011; Gao et al., 2012), indicating our lack of understanding on how dryland ecosystems respond to water stress and its relief.

Besides water availability, NEE in arid and semiarid ecosystems is also affected by other abiotic and biotic factors. Drought stress often accompanies thermal and irradia-

tion stresses, as the cloudiness is usually low and the soil is readily heated up by solar radiation during dry periods. High leaf temperature can deactivate photosystem II, enhance the evaporative demand for plants and stimulate respiration (Fu et al., 2006). Strong irradiation is common in arid and semiarid areas, and is likely to induce midday
5 photosynthetic depression (Fu et al., 2006). In many ecosystems, canopy development (e.g., changes in LAI) is critical to the seasonal evolution of CO_2 fluxes (Xu and Baldocchi, 2004; Li et al., 2005). However, the large stochasticity of PPT and variability of soil moisture in arid and semiarid ecosystems can obscure the effects of LAI (Wang et al., 2008). Considering the inconsistent effects of these environmental stresses and
10 biotic factors on CO_2 fluxes (e.g., Fu et al., 2006; Aires et al., 2008; Wang et al., 2008), it is needed to examine the relative importance of these biophysical controls and their interactions in desert shrub ecosystems.

China is one of the most threatened countries by desertification. Extensive revegetation and conservation practices have been carried out in northern China (Li et al.,
15 2004). However, little has been done to quantify the C sequestration potential of the recovering vegetation (Gao et al., 2012). Shrubland ecosystems at the south edge of the Mu Us desert lie in a critical geographic transition zone between arid and semiarid climates, and between agricultural and pastoral land uses. Overgrazing on the natural shrublands and steppes caused severe desertification in this region (Chen and Duan,
20 2009). Grazing of natural vegetation has been prohibited since the late 1990s. Thus, the vegetation has been recovering for over ten years. The rehabilitation of desertified lands has been evidenced by the increasingly fine soil texture, increased nutrient contents and biodiversity, and reduced wind erosion (Chen and Duan, 2009). The ability of the recovering ecosystems to sequester CO_2 has not yet been assessed. This
25 information, however, is essential to adaptive management under changing climate.

Using the eddy-covariance technique, we measured NEE over a shrub ecosystem at the south edge of the Mu Us desert throughout 2012. Our objectives were (1) to quantify NEE and its partitioning into GEP and R_e at diurnal, seasonal and annual scales, (2) to examine the dependence of NEE and its components on abiotic and biotic factors

BGD

11, 5089–5122, 2014

Biophysical controls on NEE over a semiarid shrubland

X. Jia et al.

Title Page

Abstract | Introduction

Conclusions | References

Tables | Figures

|◄ | ►|

◄ | ►

Back | Close

Full Screen / Esc

Printer-friendly Version

Interactive Discussion

at multiple timescales. We hypothesized that soil water shortage is dominant over other stresses in controlling NEE of dryland ecosystems, and could modify the responses of NEE to other environmental factors. We also proposed that the seasonal dynamics of LAI is an important determinant of productivity over the growing season, whereas at shorter timescales (e.g., hourly) abiotic stresses could impose critical constraints on CO_2 fluxes.

2 Materials and methods

2.1 Study site

NEE measurements were made at the Yanchi Research Station ($37°42.51′$ N, $107°13.62′$ E, 1530 m a.s.l.), Ningxia, northwest China. The area is located in the mid-temperate zone and characterized by a semiarid continental monsoon climate. The mean annual temperature (1954–2004) is 8.1 °C and the frost-free season lasts for 165 days on average (Chen and Duan, 2009; Wang et al., 2014). The mean annual PPT is 287 mm, 62 % of which falls from July to September (Feng et al., 2013). The mean annual potential evapotranspiration is 2024 mm. The soil is sandy and has a bulk density of 1.54 ± 0.08 g cm^{-3} (mean ± standard deviation (SD), $n = 16$) in the upper 10 cm of the soil profile. The area is dominated by a mixture of deciduous shrub species including *Artemisia ordosica*, *Hedysarum mongolicum* and *Hedysarum scoparium*, and also has sparsely distributed patches of *Salix psammophila* and *Agropyron cristatum*. The canopy height is about 1.4 m. Water deficit is a limiting factor for plant photosynthesis and soil respiration (R_s) at the study site (Feng et al., 2013; Wang et al., 2014).

2.2 Eddy flux measurements

The eddy-covariance instrument was mounted at a height of 6.2 m on a scaffold tower and oriented in the prevailing wind direction (northwest). A 3-D ultrasonic anemometer (CSAT3, Campbell Scientific Inc., USA) was used to measure fluctuations in wind

X. Jia et al.

speed, direction and sonic temperature. A closed-path fast response infrared gas ana-
lyzer (LI-7200, LI-COR Inc., USA) was used to measure fluctuations in CO_2 and water
vapor concentrations. The tube between the air inlet and the Li-7200 was 100 cm, the
tube flow rate was $15.0 \, L \, min^{-1}$. The tube inlet was situated about 14 cm south of, 16 cm
east of, and 8 cm below the anemometer sampling volume. We calibrated the LI-7200
every three months, using 99.99 % nitrogen gas to calibrate zeros for both CO_2 and
water vapor, and using a 650 ppm CO_2 standard and a dew point generator (LI-610,
LI-COR Inc., USA) to calibrate the span for CO_2 and water vapor, respectively. A data
logger (LI-7550, LI-COR Inc., USA) was used to store 10 Hz real-time data. The un-
derlying surface of the shrubland was flat and extended over 250 m in all directions.
Footprint analysis using the flux source area model (FASM) (Schmid, 1997) showed
that > 90 % of the fluxes originated from within 200 m of the tower. The CO_2 storage
term was not added in estimating NEE because of the short canopy (1.4 m) that usually
makes the term negligible (Zhang et al., 2007). In addition, CO_2 storage term tends to
be close to zero when summed to daily and annual timescales (Baldocchi, 2003).

2.3 Meteorological measurements

Incident photosynthetically active radiation (PAR) was measured using a quantum sen-
sor (PAR-LITE, Kipp & Zonen, the Netherlands). Net radiation (R_n) was measured using
a four-component radiometer (CNR-4, Kipp & Zonen, the Netherlands). Air temperature
(T_a) and relative humidity (RH) were measured with a thermohygrometer (HMP155A,
Vaisala, Finland). All these meteorological sensors were mounted on the tower at 6 m
aboveground. Soil temperature (T_s) and water content (SWC) profiles were monitored
adjacent to the tower using ECH_2O-5TE sensors (Decagon Devices, USA) at four
depths (0.1, 0.3, 0.7 and 1.2 m). Five soil heat plates (HFP01, Hukseflux Thermal Sen-
sors, the Netherlands) were placed at 10 cm below the soil surface, within about 5 m of
the tower base. PPT measurements started from 15 May 2012 using a tipping bucket
rain gauge (TE525WS, Campbell Scientific Inc., USA) at a distance of about 50 m from
the tower. All micrometeorological variables were measured every 10 s and then aver-

aged or summed to the 30 min resolution before being stored on data loggers (CR200X for PPT, CR3000 for all others, Campbell Scientific Inc., USA).

2.4 LAI measurements

For measuring LAI, we deployed a 4 × 4 grid of 16 quadrats (10 m × 10 m each) within a 100 m × 100 m plot centered on the flux tower in late March 2012. LAI was measured at roughly weekly intervals. The starting and ending dates for LAI measurements were specified for each species based on phenological observations. The plot-level LAI was calculated as the sum over all component species. The methods for LAI measurements were detailed in the Supplement.

2.5 Data processing and analysis

2.5.1 Flux calculation

Raw data were processed using the EddyPro 4.0.0 software (LI-COR Inc., USA). Processing steps included spike removal, tilt correction (double axis rotation), correction for sensor separation, spectral correction, detrending (Reynolds averaging) and flux computation (Burba and Anderson, 2010). Correction for density fluctuations (WPL terms) was not used, however, as LI-7200 is capable of outputting CO_2 mixing ratios, i.e., thermal expansion and water dilution of the sampled air have already been accounted for (Burba and Anderson, 2010). Half-hourly fluxes were rejected if missing records, removed spikes and absolute limit violations together exceeded 10 % of the total records of any of the three components of wind velocity and/or CO_2 concentration. CO_2 fluxes were also excluded from analyses when turbulent mixing was low during calm nights (friction velocity $u^* < 0.18\,\mathrm{m\,s^{-1}}$). The u^* threshold was estimated following the ChinaFLUX standard method (Zhu et al., 2006). Half-hourly CO_2 fluxes were despiked following Papale et al. (2006). Instrument malfunction, power failure and sensor calibration together led to 3 % missing of half-hourly flux data in 2012, while the

data quality control procedure rejected 29 % of the annual dataset. Downward fluxes are counted as negative and upward fluxes as positive. The overall performance of the eddy flux measurement system was evaluated by the degree of energy balance closure (Li et al., 2005), which was 78 % in 2012 when taking into account the heat stored in the soil above soil heat plates.

2.5.2 Gap-filling and partitioning NEE into GEP and R_e

Linear interpolation was used to fill small gaps ($\leq$ 2 h). For larger gaps during daytime (i.e., PAR $\geq$ 5 µmol m^{-2} s^{-1}), NEE-PAR relationships were used for gap-filling. A light response model (Eq. 1) which incorporates photoinhibition at high radiation (Ye, 2007) was used to estimate missing daytime data because net CO_2 uptake declined at high PAR, especially in summer (Fig. 2).

$$\text{NEE}_{\text{day}} = \alpha \frac{1 - \beta Q}{1 + \gamma Q}(Q - Q_c) \tag{1}$$

where NEE_{day} is daytime NEE (µmol CO_2 m^{-2} s^{-1}), Q is incident PAR in units of µmol m^{-2} s^{-1}, Q_c is the light compensation point, and α, β, γ are fit values for the following calculations (Ye, 2007).

$$Q_m = \frac{\sqrt{(\beta + \gamma)(1 + \gamma Q_c)/\beta} - 1}{\gamma} \tag{2}$$

$$\text{NEE}_{\text{max}} = \alpha \frac{1 - \beta Q_m}{1 + \gamma Q_m}(Q_m - Q_c) \tag{3}$$

$$\phi_0 = P'(Q = 0) = \alpha[1 + (\gamma + \beta)Q_c] \tag{4}$$

$$\phi_c = P'(Q_c) = \alpha \frac{1 + (\gamma - \beta)Q_c - \beta \gamma Q_c^2}{(1 + \gamma Q_c)^2} \tag{5}$$

$$R_d = -P(Q = 0) = -\alpha Q_c \tag{6}$$

In Eqs. (2)–(6), Q_m is the PAR intensity at the maximum rate of net CO_2 uptake (NEE_{max}), ϕ_0 and ϕ_c are the quantum yield at $Q = 0$ and $Q = Q_c$, respectively, R_d is the model-derived bulk ecosystem respiration. For the estimation of missing NEE_{day}, Eq. (1) was fit to consecutive windows of 500 non-missing daytime data points.

The Q_{10} model was used for filling nighttime gaps (Zha et al., 2004):

$$NEE_{night} = R_{e10}Q_{10}^{(T_s-10)/10} \tag{7}$$

where NEE_{night} is nighttime NEE, T_s the soil temperature at 10 cm depth, R_{e10} the R_e at $T_s = 10$, Q_{10} the temperature sensitivity of ecosystem respiration. Equation (7) was only fit to the annual dataset because short-term data points were too scattered to establish any valid $NEE_{night} - T_s$ relationships. T_s at the 10 cm depth was selected because it produced a higher coefficient of determination (R^2) than T_s at other depths and T_a. In order to estimate annual CO_2 fluxes, missing T_s values were gap-filled with the mean diurnal variation (MDV) method (Moffat et al., 2007), while missing PAR values were gap-filled using an empirical relationship to half-hourly PAR data from a meteorological tower about 3 km east.

Daytime R_e during the growing season was extrapolated from the temperature response function for NEE_{night} (Eq. 7). Off-season R_e was considered as 24 h NEE fluxes. GEP was estimated as:

$$GEP = R_e - NEE \tag{8}$$

2.5.3 Statistical analysis

Equation (1) was fit monthly from May to October to evaluate the seasonal variation in light response of NEE. The regressions were conducted on bin-averaged data using 50 µmol m^{-2} s^{-1} PAR intervals. In order to test the dependency of the NEE_{day}–PAR relationship on abiotic factors and exclude the confounding effects of plant phenology, we compiled NEE_{day} during the peak growing season (June–August) into multiple groups

according to VPD (VPD ≤ 1 kPa, 1 kPa $<$ VPD ≤ 2 kPa, VPD > 2 kPa), T_a ($T_a \leq 20\,^{\circ}$C, $20\,^{\circ}$C $< T_a \leq 25\,^{\circ}$C, $T_a > 25\,^{\circ}$C) and SWC at 30 cm depth (SWC $\leq 0.1\,\text{m}^3\,\text{m}^{-3}$, SWC $> 0.1\,\text{m}^3\,\text{m}^{-3}$). The NEE$_{\text{day}}$ values were then bin-averaged before parameters were fit for each group. To evaluate the relative importance of different abiotic factors, Eq. (1) was fit to all half-hourly NEE$_{\text{day}}$ values during June–August, and the residuals were then subjected to least-square regressions and a stepwise multiple linear regression against VPD, T_a and SWC (Z-transformed data were used in the stepwise regression). In order to test NEE$_{\text{day}}$–T_a and NEE$_{\text{day}}$–VPD relationships, as well as their dependence on SWC, NEE$_{\text{day}}$ was compiled with respect to SWC at 30 cm depth (SWC $\leq 0.1\,\text{m}^3\,\text{m}^{-3}$, SWC $> 0.1\,\text{m}^3\,\text{m}^{-3}$), and then bin-averaged into $1\,^{\circ}$C T_a and 0.2 kPa VPD intervals, respectively. NEE$_{\text{day}}$–T_a and NEE$_{\text{day}}$–VPD relationships were fit with the quadratic model.

For examining the effects of SWC on the R_e–T_s (10 cm depth) relationship, we classified NEE$_{\text{night}}$ when $T_s > 0\,^{\circ}$C into two groups with respect to SWC at 30 cm depth (SWC $\leq 0.1\,\text{m}^3\,\text{m}^{-3}$, SWC $> 0.1\,\text{m}^3\,\text{m}^{-3}$), and then bin-averaged NEE$_{\text{night}}$ into $1\,^{\circ}$C T_s intervals. R_{e10} and Q_{10} in Eq. (7) were estimated separately for each SWC group. A minimum of ten data points were required for a valid bin for all abovementioned bin-averages. The following surface fitting (T_s-REW model) was then used to further examine the interaction between temperature and water availability in regulating half-hourly NEE$_{\text{night}}$:

$$\text{NEE}_{\text{night}} = (a + b\,\text{REW})(c + d\,\text{REW})^{(T_s - 10)/10} \tag{9}$$

where a, b, c and d are fit parameters. REW means relative extractable water content (Zhou et al., 2013), which was calculated as:

$$\text{REW} = \frac{\text{SWC} - \text{SWC}_{\text{min}}}{\text{SWC}_{\text{max}} - \text{SWC}_{\text{min}}} \tag{10}$$

where SWC$_{\text{max}}$ and SWC$_{\text{min}}$ are the minimum and maximum SWC during the period of $T_s > 0\,^{\circ}$C, respectively. Linear regressions were used to compare measured vs. predicted half-hourly NEE$_{\text{night}}$ values and to examine the dependence of NEE$_{\text{night}}$ residuals

on REW for both the Q_{10} model (Eq. 7) and the T_s-REW model (Eq. 10). SWC at 30 cm depth was chosen for both daytime and nighttime analyses because its effects were most pronounced among SWC at different layers.

Linear regressions were used to examine the seasonal relationships between GEP and R_e, and the responses of NEE and GEP to seasonal changes in LAI. For this purpose, daily-integrated values were calculated for C fluxes, and daily LAI was derived by linear interpolation between measurements. The uncertainty for annual fluxes were estimated by bootstrapping, in which the gap-filled annual dataset was sampled 2000 times and then SD calculated (applied to half-hourly data).

3 Results

3.1 Seasonal variation in environmental conditions

Environmental variables showed clear seasonal patterns (Fig. 1). The daily mean T_a ranged from −8.5 on 23 January to 23.4 °C on 11 July (Fig. 1a). T_s had a minimum of −12.1 °C on 8 February and a maximum of 25.8 °C on 22 June (Fig. 1a). The daily PAR reached a maximum of 61.5 mol m^{-2} day^{-1} on 15 June, and was < 30 mol m^{-2} day^{-1} during winter (Fig. 1b). Daily mean VPD reached a maximum of 2.2 kPa on 9 June, and was lower than < 0.5 kPa during winter (Fig. 1c). PPT summed to 304.9 mm from mid-May to December, > 60 % of which fell between June and August. There were three rain events larger than 20 mm day^{-1}, among which the largest occurred on 27 June (49.8 mm day^{-1}) (Fig. 1d). Snowmelt and soil thaw in early spring resulted in a relatively wet soil (Fig. 1d). During the growing season, SWC (except for that at 120 cm depth) followed the pattern of precipitation, and SWC in deeper layers (30 and 70 cm) only responded to large rainfall events (Fig. 1d).

3.2 Seasonal variation in NEE and its biophysical controls

Daily NEE ranged from $-4.71\,\mathrm{g\,C\,m^{-2}\,day^{-1}}$ (largest net CO_2 uptake) on 30 June to $1.63\,\mathrm{g\,C\,m^{-2}\,day^{-1}}$ on 30 July (Fig. 1f). GEP reached a maximum of $6.78\,\mathrm{g\,C\,m^{-2}\,day^{-1}}$ on 30 June. Maximum R_e was $3.26\,\mathrm{g\,C\,m^{-2}\,day^{-1}}$ on 25 July. Annual net ecosystem productivity (NEP = $-$NEE) was 77 ± 7 (SD) $\mathrm{g\,C\,m^{-2}\,yr^{-1}}$. R_e contributed $379\pm3\,\mathrm{g\,C\,m^{-2}\,yr^{-1}}$ to NEP, leading to an annual GEP of $456\pm8\,\mathrm{g\,C\,m^{-2}\,yr^{-1}}$.

PAR was the direct control over $\mathrm{NEE_{day}}$ during the growing season (Fig. 2), accounting for $>80\%$ of the variability in $\mathrm{NEE_{day}}$ in most months (except for October) (Table 1). The absolute values of $\mathrm{NEE_{max}}$, ϕ_0, ϕ_c and R_d were all highest in July, while lower in spring and autumn (Table 1). The direct effect of PAR was modified by other environmental factors (Table 2; Fig. 3). The magnitude of $\mathrm{NEE_{max}}$ and ϕ_c decreased, while Q_m increased, with increasing VPD and T_a. In addition, R_d increased with T_a. The magnitude of $\mathrm{NEE_{max}}$, Q_m and R_d were all lower under dry soil conditions. The $\mathrm{NEE_{day}}$ residuals were positively correlated with VPD and T_a, and negatively correlated with SWC (Fig. 3d–f). The stepwise regression produced the following relationship: residual $= -0.30\mathrm{SWC} + 0.17T_a + 0.11\mathrm{VPD}$ ($R^2 = 0.16$, $P < 0.01$).

$\mathrm{NEE_{day}}$ first decreased (towards higher CO_2 uptake), and then increased, with increasing T_a and VPD (Fig. 4). Moreover, $\mathrm{NEE_{day}}$ was more responsive to T_a and VPD, and showed higher maximum CO_2 uptake rates under wetter soil conditions (SWC $\geq 0.1\,\mathrm{m^3\,m^{-3}}$). For most of the VPD range, $\mathrm{NEE_{day}}$ was more negative under higher soil water availability (Fig. 4b).

$\mathrm{NEE_{night}}$ showed close relationships with T_s at 10 cm depth for both SWC groups (Fig. 5). However, Q_{10} was much larger, and R_{e10} slightly smaller, under higher soil water availability. The surface fitting showed that Q_{10} increased from 1.9 to 3.2, and R_{e10} increased with from 0.73 to $0.83\,\mathrm{\mu mol\,m^{-2}\,s^{-1}}$, when REW increased from 0 to 1 (Fig. 6). The T_s-REW model fit the measured half-hourly values better than the Q_{10} model (Fig. 7). Half-hourly $\mathrm{NEE_{night}}$ residuals showed a positive correlation with REW

(Fig. 7b). However, the pattern disappeared after incorporating REW into the model (Fig. 7d).

There was a linear dependence of daily R_e on GEP ($R^2 = 0.65$), with a slope of 0.34 (Fig. 8a). Both daily GEP and NEE responded to the seasonal variation of LAI ($R^2 = 0.65$ and 0.45, respectively), with a slope of 4.12 for GEP, and −2.03 for NEE (Fig. 8b and c).

3.3 Synoptic variation in NEE as related to rain pulses

Pulses of NEE were observed during the growing season when precipitation occurred (Fig. 9a). In order to examine the effects of rain events and related environmental factors on NEE, half-hourly measurements around the largest rainfall event (DOY 179–180, 61 mm) were scrutinized (Fig. 9b and c). NEE during daytime was markedly depressed on DOY 179–180 compared to the day before rain (DOY 178), and NEE during nighttime was slightly higher on DOY 179–180 than on days without rain (DOY 181–184). As a result, a positive pulse in daily NEE was observed on DOY 179–180 (Fig. 9a). The positive NEE pulse was accompanied by a sharp increase in SWC, and decreases in T_a, T_s and PAR (Fig. 9b and c). Daytime NEE was dramatically stimulated by high PAR, temperatures and SWC on days immediately following the rain event (DOY 181–182), leading to a clear post-rain peak in CO_2 uptake.

3.4 Diurnal variations in NEE and meteorological factors

The monthly mean diurnal variations of non-rainy days showed that the diel amplitude of NEE varied dramatically over the growing season, being largest in July and smallest in October (Fig. 10a). NEE during nighttime was relatively low in magnitude in comparison to that during daytime in most months (except for October). As a result, the ecosystem was a C sink on non-rainy days from May to September. Net CO_2 uptake peaked before noon (at 09:30–10:00 LST, LST = GMT + 8) in summer months (June–August), leading to an asymmetric distribution of NEE around noon. PAR did not show

such an asymmetry, being highest between 12:30 and 13:30 LST (GMT + 8) (Fig. 10b). Both T_a and VPD were lowest in early morning, and peaked in late afternoon (Fig. 10c and d).

4 Discussion

4.1 Magnitude of NEP

Dryland ecosystems can vary from a net sink to source of CO_2 on an annual basis, as mainly determined by water availability and the amount of primary producers (Liu et al., 2012). The total amount of C sequestered by the studied shrubland in 2012 (NEP = $77 \pm 7\,\mathrm{g\,C\,m^{-2}\,yr^{-1}}$), with an annual PPT of at least 305 mm and a peak LAI of 1.2, was generally lower than that by forests and grasslands in humid and subhumid areas (e.g., Suyker and Verma, 2001; Zha et al., 2004; Zhou et al., 2013). However, it was higher than many reported values from semiarid and arid nonforest ecosystems (Wang et al., 2008; Gao et al., 2012). For example, a revegetated shrub ecosystem $\sim 200\,\mathrm{km}$ west of our site dominated by *Caragana korshinskii* and *A. ordosica* had a NEP of $14\text{–}23\,\mathrm{g\,C\,m^{-2}\,yr^{-1}}$, with an annual PPT of $< 150\,\mathrm{mm}$ (Gao et al., 2012). An semiarid steppe in central Mongolia showed a NEP of $41\,\mathrm{g\,C\,m^{-2}\,yr^{-1}}$, an annual PPT of 260 mm and a peak LAI of 0.57 (Li et al., 2005). Liu et al. (2012) reported that a salt desert shrubland (with LAI < 0.4) in northwest China was near C neutral in a dry year (PPT = 17 mm), but a C sink of $40\,\mathrm{g\,C\,m^{-2}\,yr^{-1}}$ in a wet year (PPT = 48 mm). The shrub ecosystem we studied has a wide regional distribution, thus represents a huge C fixation potential. At our site, PPT in 2012 was at least 18 mm higher than the long-term mean, which calls for future studies that assess how semiarid shrub ecosystems respond to interannual variability in water availability.

4.2 Effects of abiotic stresses on NEE

The nature and relative importance of different biophysical factors in controlling NEE differ among ecosystem types (Fu et al., 2006). Water stress, which has the largest seasonal and interannual variation among all environmental variables, is the most common limitation to vegetation growth in dryland ecosystems (Fu et al., 2006). Our study also revealed the dominant role of soil water in limiting photosynthesis. Fu et al. (2006) found that water stress was responsible for photosynthetic depression in a semiarid steppe, while high temperature together with strong solar radiation caused a decrease of NEE_{day} in an alpine shrub. Our findings that low SWC and high VPD depressed the maximum rate of CO_2 uptake (NEE_{max}) (Table 2; Fig. 3) were in agreement with previous studies in dryland ecosystems (Li et al., 2005; Wang et al., 2008; Yang et al., 2011). Both SWC and VPD affect plant hydraulic status, however, they reduce C assimilation through different mechanisms. Dry soil leads to reduced water supply for metabolism and cell expansion, while VPD affects CO_2 supply for photosynthesis by regulating stomatal conductance and evaporative demand (Zhou et al., 2013). Moreover, the two mechanisms did not act in isolation, but interacted to reduce CO_2 uptake under water-stressed conditions (Fig. 4). Li et al. (2005) concluded that the sensitivity of stomata to VPD becomes stronger once leaf water potential starts to drop because of deficiency of water supply from the soil. Low soil water availability may aggravate VPD-induced stomatal closure.

Water limitation of R_e or R_s has been found in various types of ecosystems (Gao et al., 2012). Our results showed a marked decrease in both the magnitude and temperature sensitivity (Q_{10}) of R_e under low SWC (Figs. 5 and 6). Wang et al. (2014) measured R_s in a nearby community dominated by *A. ordosica* (800 m north of the eddy-flux tower), and found that R_s was closely correlated with T_s when SWC at 10 cm depth was higher than $0.08\,\mathrm{m^3\,m^{-3}}$, while it was decoupled from temperature during dry periods. The reduction in Q_{10} of R_e under drought conditions was most likely associated with decreased C transportation to roots due to suppressed photosynthesis,

Title Page

Abstract | Introduction

Conclusions | References

Tables | Figures

|◄ | ►|

◄ | ►

Back | Close

Full Screen / Esc

Printer-friendly Version

Interactive Discussion

inactivated rhizosphere and switched C pool being respired (e.g., from labile to recalcitrant) (Zhang et al., 2007; Wang et al., 2008; Gao et al., 2012).

Air temperature is another factor affecting VPD besides humidity, which could explain the reduction in NEE_{max} at high temperatures (Fig. 3b). Alternatively, high T_a might have enhanced respiration and/or suppressed photosystem II, resulting in smaller NEE_{max}. The quadratic relationship between NEE_{day} and T_a was likely due to PAR-limited C assimilation on cloudy and rainy days at low temperatures, and to heat- and water-limited NEE_{day} at high temperatures (Fu et al., 2006). Similar to Li et al. (2005), we found that NEE_{day} became less responsive to T_a under drought conditions (Fig. 4a), reflecting drought limitations to both plant and microbial activities. A downward shift of optimum T_a of NEE_{day} under low SWC was attributable to different responses of GEP and R_e to water deficit (Fu et al., 2006). The asymmetric distribution of net photosynthesis around noon (Fig. 10a) is commonly observed in arid areas (Zhang et al., 2007), and can be ascribed to either temperature-induced increases in R_e (Fig. 10c) or VPD-induced stomatal closure (Fig. 10d) in the afternoon (Yang et al., 2011). The strong solar radiation at our site (Figs. 1 and 2) led to decreases in CO_2 uptake in summer months (Figs. 2 and 3). Insufficient thermal dissipation of leaves and consequent damage of photosynthetic apparatus are the likely causes for photoinhibition of CO_2 assimilation (Fu et al., 2006).

4.3 Effects of rain pulses on NEE

Rain events triggered pulsed dynamics of NEE in the shrub ecosystem during the growing period (Fig. 9a). Large positive daily NEE occurred immediately after a rainfall event, but the peak of CO_2 uptake lagged the pulse of CO_2 release by 1–2 days (Fig. 9a and b). Similarly, Gao et al. (2012) found that a large precipitation event resulted in a rapid burst of positive C flux (CO_2 release) before negative values set in 1–2 days later in a revegetated shrubland in northwest China. Wang et al. (2014) also reported immediate pulses of R_s following rain events in an *A. ordosica* dominated community at our site. In a semiarid steppe in central Mongolia, the respiration enhancement effect

was even higher during the rain period itself (Li et al., 2005). In contrast, Liu et al. (2011) found in a saline desert that NEE took 4–5 days to reach its peak of CO_2 uptake after rain. The rapid stimulation of CO_2 release by precipitation may arise from the rapid activation of microorganisms and decomposition of soil organic matter due to the "Birch effect", which has been widely reported in regions with dry soils when a rainfall event occurs after a period of drought (Jarvis et al., 2007). Alternatively, soil water from rainfall may have degassed the CO_2 stored in soil pores, considering the sandy soils with high porosity in desert areas (Lee et al., 2004). The lagged responses of photosynthesis may be associated with physiological acclimation and recovery of plants from the preceding dry period (Liu et al., 2011), and related to the post-rainfall environmental conditions that are optimum for C assimilation (Fig. 9c). These results showed that fast and slow responses together contribute to the pulsed ecosystem behavior.

4.4 Biotic controls on CO_2 fluxes

Leaf area represents both the amount of photosynthetic tissues and the amount of intercepted light by the vegetation (Yang et al., 2011). Our results that photosynthetic parameters varied seasonally (Table 2; Fig. 2) with canopy development (e.g., changes in LAI) has been reported previously for different vegetations (Zha et al., 2004; Yang et al., 2011). Furthermore, we found that LAI accounted for 45 and 65 % of the seasonal variation in NEE and GEP, respectively (Fig. 8b and c), indicating the importance of canopy development in controlling C balance. Similar GEP-LAI and NEE-LAI relationships have been reported for steppe, grassland and pasture ecosystems (e.g., Tappeiner and Cernusca, 1998, Flanagan et al., 2002; Yang et al., 2011). The slope of the GEP-LAI relationship reported here ($4.1\,\mathrm{g\,C\,(m^2\,leaf\,area)^{-1}\,day^{-1}}$) was comparable to that in a semiarid steppe ($3.1\,\mathrm{g\,C\,m^{-2}\,day^{-1}}$) (Li et al., 2005) and two Mediterranean grasslands (3.9–$4.1\,\mathrm{g\,C\,m^{-2}\,day^{-1}}$, Xu and Baldocchi, 2004; Aires et al., 2008). However, it was much smaller than that (7.5–$8.7\,\mathrm{g\,C\,m^{-2}\,day^{-1}}$) found in a Canadian temperate grassland (Flanagan et al., 2002). A small GEP-LAI slope may be indicative of water and nutrient limitations (Li et al., 2005).

Title Page

Abstract | Introduction

Conclusions | References

Tables | Figures

|◄ | ►|

◄ | ►

Back | Close

Full Screen / Esc

Printer-friendly Version

Interactive Discussion

Canopy productivity was shown to have a shadowing effect on R_e as photosynthesis provides substrates to both autotrophic and heterotrophic respiration (Wan and Luo, 2003; Flanagan and Johnson, 2005). In our study, GEP accounted for 65 % of the seasonal variation in R_e, with a slope of 0.34 (Fig. 8a). Li et al. (2005) reported a similar slope (0.33) for the R_e–GEP relationship in a semiarid steppe. Xu and Baldocchi (2004) and Aires et al. (2008) showed slopes of 0.47 and 0.53 in Mediterranean grasslands, respectively. However, Liu et al. (2011) reported a larger slope (0.8) in a saline desert shrub ecosystem, which may reflect greater C allocation to respiratory tissues (stems, branches and coarse roots) or functions (e.g., maintenance respiration).

5   Conclusions

In line with our hypotheses, we found in the semiarid shrub ecosystem that (1) water stress exerted a major control over half-hourly changes in NEE during the peak growing season, and interacted with heat stress and photoinhibition in constraining C fixation; (2) rain pulses regulated NEE at the synoptic scale, highlighting the role of water supply in the alleviation of abiotic stresses; (3) canopy development largely determined NEE and GEP over the entire growing season. Climate modeling suggests a warmer and drier future climate in the semiarid and arid regions of Asia (McCarthy et al., 2001). Hence, more stressful environmental conditions in the future may lead to substantially lower carbon sequestration capacity in temperate semiarid areas. Also, the predicted higher variability in precipitation (Easterling et al., 2000), i.e., more extreme but less frequent rainfall events intervened by longer dry periods, accentuates the role of the temporal pattern of water availability in controlling NEE in the future.

Supplementary material related to this article is available online at http://www.biogeosciences-discuss.net/11/5089/2014/ bgd-11-5089-2014-supplement.pdf.

References

10 Aires, L. M. I., Pio, C. A., and Pereira, J. S.: Carbon dioxide exchange above a Mediterranean C3/C4 grassland during two climatologically contrasting years, Glob. Change Biol., 14, 539–555, 2008.

Asner, G. P., Archer, S., Hughes, R. F., Ansley, R. J., and Wessman, C. A.: Net changes in regional woody vegetation cover and carbon storage in Texas drylands, 1937–1999, Glob.
15 Change Biol., 9, 316–335, 2003.

Baldocchi, D. D.: Assessing the eddy covariance technique for evaluating carbon dioxide exchange rates of ecosystems: past, present and future, Glob. Change Biol., 9, 479–492, 2003.

Burba, G. and Anderson, D.: A Brief Practical Guide to Eddy Covariance Flux Measurements: Principles and Workflow Examples for Scientific and Industrial Applications, LI-COR Bio-
20 sciences, 2010.

Chen, X. and Duan, Z.: Changes in soil physical and chemical properties during reversal of desertification in Yanchi County of Ningxia Hui autonomous regions, China, Environ. Geol., 57, 975–985, 2009.

Easterling, D. R., Meehl, G. A., Parmesan, C., Changnon, S. A., Karl, T. R., and Mearns, L. O.:
25 Climate extremes: observations, modeling, and impacts, Science, 289, 2068–2074, 2000.

Feng, W., Zhang, Y., Wu, B., Zha, T., Jia, X., Qin, S., Shao, C., Liu, J., Lai, Z., and Fa, K.: Influence of disturbance on soil respiration in biologically crusted soil during the dry season, Sci. World J., 2013, 408560, doi:10.1155/2013/408560, 2013.

Flanagan, L. B. and Johnson, B. G.: Interacting effects of temperature, soil moisture and plant biomass production on ecosystem respiration in a northern temperate grassland, Agr. Forest Meteorol., 130, 237–253, 2005.

Flanagan, L. B., Wever, L. A., and Carlson, P. J.: Seasonal and interannual variation in carbon dioxide exchange and carbon balance in a northern temperate grassland, Glob. Change Biol., 8, 599–615, 2002.

Fu, Y. L., Yu, G. R., Sun, X. M., Li, Y. N., Wen, X. F., Zhang, L. M., Li, Z. Q., Zhao, L., and Hao, Y. B.: Depression of net ecosystem CO_2 exchange in semi-arid *Leymus chinensis* steppe and alpine shrub, Agr. Forest Meteorol., 137, 234–244, 2006.

Gao, Y., Li, X., Liu, L., Jia, R., Yang, H., Li, G., and Wei, Y.: Seasonal variation of carbon exchange from a revegetation area in a Chinese desert, Agr. Forest Meteorol., 156, 134–142, 2012.

Jarvis, P., Rey, A., Petsikos, C., Wingate, L., Reyment, M., Pereira, J., Banza, J., David, J., Miglietta, F., Borghetti, M., Manca, G., and Valentini, R.: Drying and wetting of Mediterranean soils stimulates decomposition and carbon dioxide emission: the "Birch effect", Tree Physiol., 27, 929–940, 2007.

Lal, R.: Carbon sequestration in dryland ecosystems, Environ. Manage., 33, 528–544, 2004.

Lee, X., Wu, H. J., Sigler, J., Oishi, C., and Siccama, T.: Rapid and transient response of soil respiration to rain, Glob. Change Biol., 10, 1017–1026, 2004.

Li, S. G., Asanuma, J., Eugster, W., Kotani, A., Liu, J. J., Urano, T., Oikawa, T., Davaa, G., Oyunbaatar, D., and Sugita, M.: Net ecosystem carbon dioxide exchange over grazed steppe in central Mongolia, Glob. Change Biol., 11, 1941–1955, 2005.

Li, X. R., Ma, F. Y., Xiao, H. L., Wang, X. P., and Kim, K. C.: Long-term effects of revegetation on soil water content of san dunes in arid regions of Northern China, J. Arid Environ., 57, 1–16, 2004.

Liu, R., Li, Y., and Wang, Q. X.: variations in water and CO_2 fluxes over a saline desert in western China, Hydrol. Process., 26, 513–522, 2011.

Liu, R., Pan, L. P., Jenerette, G. D., Wang, Q. X., Cieraad, E., and Li, Y.: High efficiency in water use and carbon gain in a wet year for a desert halophyte community, Agr. Forest Meteorol., 162–163, 127–135, 2012.

McCarthy, J., Canziani, O., Leary, N., Dokken, D. J., and White, K. S.: Climate Change 2001: Impacts, Adaptation, and Vulnerability, Cambridge University Press, New York, 2001.

Moffat, A. M., Papale, D., Reichstein, M., Hollinger, D. Y., Richardson, A. D., Barr, A. G., Beckstein, C., Braswell, B. H., Churkina, G., Desai, A. R., Falge, E., Gove, J. H., Heimann, M., Hui, D., Jarvis, A. J., Kattge, J., Noormets, A., and Stauch, V. J.: Comprehensive comparison of gap-filling techniques for eddy covariance net carbon fluxes, Agr. Forest Meteorol., 147, 209–232, 2007.

Papale, D., Reichstein, M., Aubinet, M., Canfora, E., Bernhofer, C., Kutsch, W., Longdoz, B., Rambal, S., Valentini, R., Vesala, T., and Yakir, D.: Towards a standardized processing of Net Ecosystem Exchange measured with eddy covariance technique: algorithms and uncertainty estimation, Biogeosciences, 3, 571–583, doi:10.5194/bg-3-571-2006, 2006.

Schmid, H. P.: Experimental design for flux measurements: matching scales of observations and fluxes, Agr. Forest Meteorol., 87, 179–200, 1997.

Suyker, A. E. and Verma, S. B.: Year-round observations of the net ecosystem exchange of carbon dioxide in a native tallgrass prairie, Glob. Change Biol., 7, 279–289, 2001.

Tappeiner, U. and Cernusca, A.: Model simulation of spatial distribution of photosynthesis in structural differing plant communities in the Central Caucasus, Ecol. Model., 113, 201–223, 1998.

Wan, S. and Luo, Y.: Substrate regulation of soil respiration in tallgrass prairie: results of a clipping and shading experiment, Global Biogeochem. Cy., 17, 1054, doi:10.1029/2002GB001971, 2003.

Wang, B., Zha, T. S., Jia, X., Wu, B., Zhang, Y. Q., and Qin, S. G.: Soil moisture modifies the response of soil respiration to temperature in a desert shrub ecosystem, Biogeosciences, 11, 259–268, doi:10.5194/bg-11-259-2014, 2014.

Wang, Y., Zhou, G., and Wang, Y.: Environmental effects on net ecosystem CO_2 exchange at half-hour and month scales over *Stipa krylovii* steppe in northern China, Agr. Forest Meteorol., 148, 714–722, 2008.

Whittaker, R. H.: Communities and Ecosystems, MacMillan publishing Co., New York, 1975.

Xu, L. and Baldocchi, D. D.: Seasonal variation in carbon dioxide exchange over a Mediterranean annual grassland in California, Agr. Forest Meteorol., 123, 79–96, 2004.

Yang, F., Zhou, G., Hunt, J. E., and Zhang, F.: Biophysical regulation of net ecosystem carbon dioxide exchange over a temperate desert steppe in Inner Mongolia, China, Agr. Forest Meteorol., 142, 318–328, 2011.

Ye, Z. P.: A new model for relationship between irradiance and the rate of photosynthesis in *Oryza sativa*, Photosynthetica, 45, 637–640, 2007.

Zha, T., Kellomäki, S., Wang, K., and Rouvinen, I.: Carbon sequestration and ecosystem respiration for 4 years in a scots pine forest, Glob. Change Biol., 10, 1492–1503, 2004.

Zhang, W. L., Chen, S. P., Chen, J., Wei, L., Han, X. G., and Lin, G. H.: Biophysical regulations of carbon fluxes of a steppe and a cultivated cropland in semiarid Inner Mongolia, Agr. Forest Meteorol., 146, 216–229, 2007.

Zhu, Z., Sun, X., Wen, X., Zhou, Y., Tian, J., and Yuan, G.: Study on the processing method of nighttime CO_2 eddy covariance flux data in ChinaFLUX, Sci. China Ser. D, 49, supp. II, 36–46, 2006.

Zhou, J., Zhang, Z., Sun, G., Fang, X., Zha, T., McNulty, S., Chen, J., Jin, Y., and Noormets, A.: Response of ecosystem carbon fluxes to drought events in a poplar plantation in Northern China, Forest Ecol. Manag., 300, 33–42, 2013.

Title Page

Abstract | Introduction

Conclusions | References

Tables | Figures

◄ | ►

◄ | ►

Back | Close

Full Screen / Esc

Printer-friendly Version

Interactive Discussion

Table 1. Parameter values describing the response of daytime NEE to incident PAR for each month and the entire growing season (GS).

Month	α (×10^3)	β (×10^4)	γ (×10^4)	Q_c	Q_m	NEE_{max}	ϕ_0	ϕ_c	R_d	Adj. R^2
May	-6.59 ± 1.65	4.01 ± 0.61	-0.04 ± 3.14	186.94 ± 36.34	1344.19	-3.54	-0.0071	-0.0061	1.23	0.82
Jun	-14.87 ± 2.18	3.04 ± 0.37	5.61 ± 2.97	141.22 ± 16.28	1340.05	-6.03	-0.0167	-0.0132	2.10	0.93
Jul	-17.67 ± 2.56	3.12 ± 0.48	3.96 ± 2.86	154.99 ± 17.23	1395.40	-7.98	-0.0196	-0.0158	2.74	0.94
Aug	-15.71 ± 3.01	3.69 ± 0.39	7.83 ± 4.47	146.00 ± 18.69	1105.94	-4.79	-0.0184	-0.0133	2.29	0.86
Sep	-7.33 ± 1.92	2.31 ± 1.79	6.23 ± 8.04	159.79 ± 23.65	1629.61	-3.33	-0.0083	-0.0064	1.17	0.90
Oct	-1.59 ± 0.93	6.59 ± 2.46	3.92 ± 18.90	324.98 ± 86.41	869.97	-0.28	-0.0021	-0.0011	0.52	0.36
GS	-11.80 ± 1.41	1.10 ± 0.58	12.20 ± 4.08	150.06 ± 9.91	2281.00	-4.98	-0.0142	-0.0098	1.77	0.96

Fit parameters in Eq. (1) (α, β, γ and Q_c) are presented as mean $\pm$ SE. NEE ($\mu mol\,CO_2\,m^{-2}\,s^{-1}$), net ecosystem CO_2 exchange; PAR ($\mu mol\,m^{-2}\,s^{-1}$), photosynthetically active radiation; Q_c ($\mu mol\,m^{-2}\,s^{-1}$), light compensation point; NEE_{max} ($\mu mol\,CO_2\,m^{-2}\,s^{-1}$), the maximum magnitude of daytime NEE; Q_m ($\mu mol\,m^{-2}\,s^{-1}$), the PAR intensity corresponding to NEE_{max}; ϕ_0 and ϕ_c ($\mu mol\,\mu mol^{-1}$), the quantum yield when PAR is equal to zero and Q_c, respectively; R_d ($\mu mol\,CO_2\,m^{-2}\,s^{-1}$), model-derived bulk ecosystem respiration; Adj. R^2, adjusted coefficient of determination.

Table 2. Parameter values describing the response of daytime NEE to incident PAR during the peak growing season (June–August) under different environmental conditions.

Treatment	α ($\times 10^3$)	β ($\times 10^4$)	γ ($\times 10^4$)	Q_c	Q_m	NEE_{max}	ϕ_0	ϕ_c	R_d	Adj. R^2
VPD ≤ 1	-14.46 ± 1.58	5.18 ± 0.47	-2.58 ± 1.46	152.80 ± 17.76	1184.57	-8.30	-0.0150	-0.0139	2.21	0.96
$1 < VPD \leq 2$	-15.33 ± 2.84	2.61 ± 0.55	6.28 ± 4.07	150.00 ± 20.32	1482.84	-6.49	-0.0174	-0.0135	2.30	0.90
VPD > 2	-13.86 ± 6.81	0.89 ± 1.49	17.85 ± 17.80	150.20 ± 33.65	2332.48	-4.64	-0.0178	-0.0108	2.08	0.80
$T_a \leq 20$	-16.10 ± 2.47	3.91 ± 0.63	1.48 ± 2.84	146.88 ± 19.01	1260.76	-7.65	-0.0174	-0.0149	2.36	0.94
$20 < T_a \leq 25$	-17.35 ± 3.27	2.99 ± 0.49	6.42 ± 4.11	150.83 ± 20.22	1334.66	-6.64	-0.0198	-0.0151	2.62	0.89
$T_a > 25$	-13.96 ± 8.36	1.77 ± 1.17	12.00 ± 15.1	208.20 ± 50.47	1763.11	-4.79	-0.0180	-0.0108	2.91	0.79
SWC ≤ 0.1	-17.63 ± 3.13	3.06 ± 0.36	9.62 ± 4.39	129.53 ± 17.06	1204.58	-5.54	-0.0205	-0.0151	2.28	0.88
SWC > 0.1	-16.61 ± 2.38	2.84 ± 0.48	4.05 ± 2.84	177.30 ± 17.22	1512.46	-7.85	-0.0186	-0.0147	2.94	0.94

Fit parameters in Eq. (1) (α, β, γ and Q_c) are presented as mean ± SE. NEE ($\mu mol\,CO_2\,m^{-2}\,s^{-1}$), net ecosystem CO_2 exchange; PAR ($\mu mol\,m^{-2}\,s^{-1}$), photosynthetically active radiation; Q_c ($\mu mol\,m^{-2}\,s^{-1}$), light compensation point; NEE_{max} ($\mu mol\,CO_2\,m^{-2}\,s^{-1}$), the maximum magnitude of daytime NEE; Q_m ($\mu mol\,m^{-2}\,s^{-1}$), the PAR intensity corresponding to NEE_{max}; ϕ_0 and ϕ_c ($\mu mol\,\mu mol^{-1}$), the quantum yield when PAR is equal to zero and Q_c, respectively; R_d ($\mu mol\,CO_2\,m^{-2}\,s^{-1}$), model-derived bulk ecosystem respiration; Adj. R^2, adjusted coefficient of determination; VPD (kPa), vapor pressure deficit; T_a (°C), air temperature at 6 m aboveground, SWC ($m^3\,m^{-3}$), soil water content at 30 cm depth.
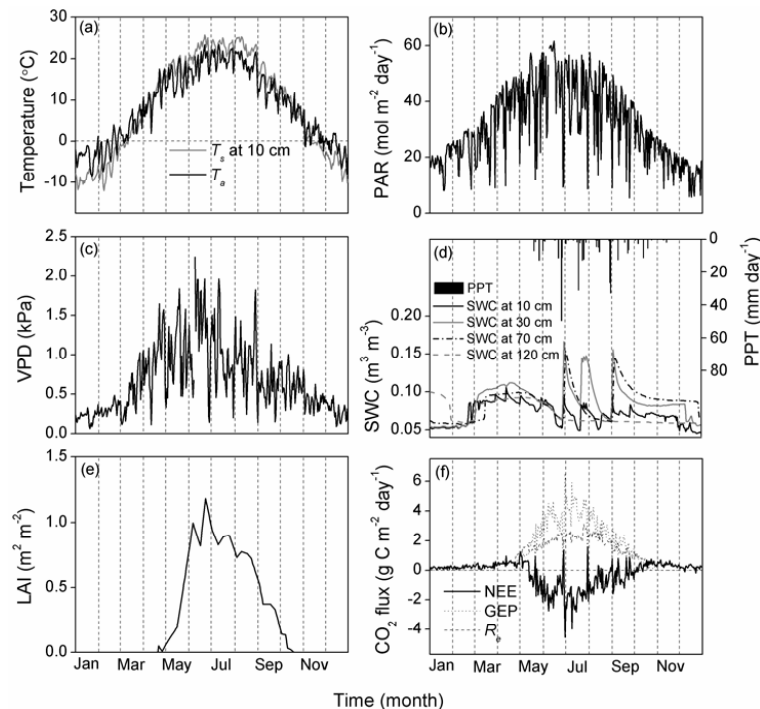
Fig. 1. Seasonal variations of air temperature (T_a) at 6 m aboveground and soil temperature (T_s) at 10 cm depth **(a)**, incident photosynthetically active radiation (PAR) **(b)**, vapor pressure deficit (VPD) **(c)**, soil water content (SWC) and precipitation (PPT) **(d)**, leaf area index (LAI) **(e)** and CO_2 fluxes **(f)** in 2012. NEE, net ecosystem CO_2 exchange; GEP, gross ecosystem productivity; R_e, ecosystem respiration. Daily means are shown for T_a, T_s, VPD and SWC; Daily sums are shown for PAR, PPT and CO_2 fluxes; interpolated daily values are shown for LAI. The vertical dashed lines separate each month, and the horizontal dashed lines in **(a)** and **(f)** represent $y = 0$.
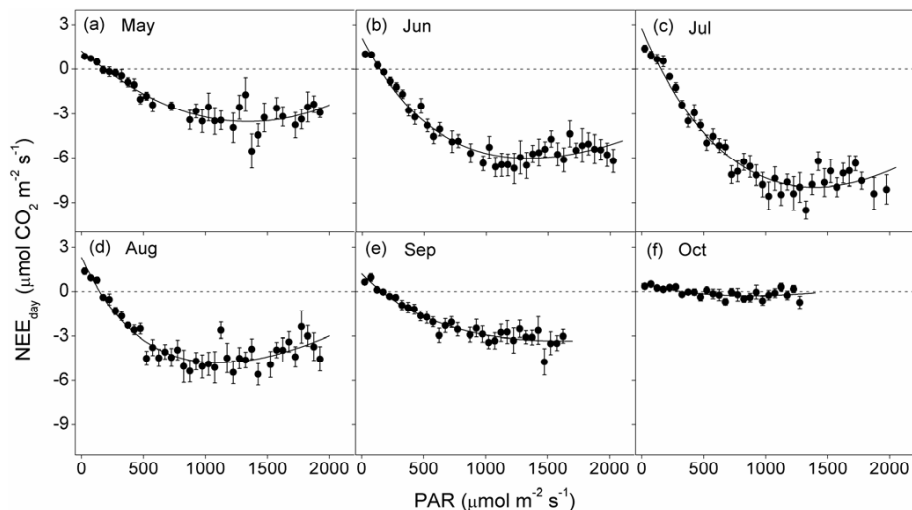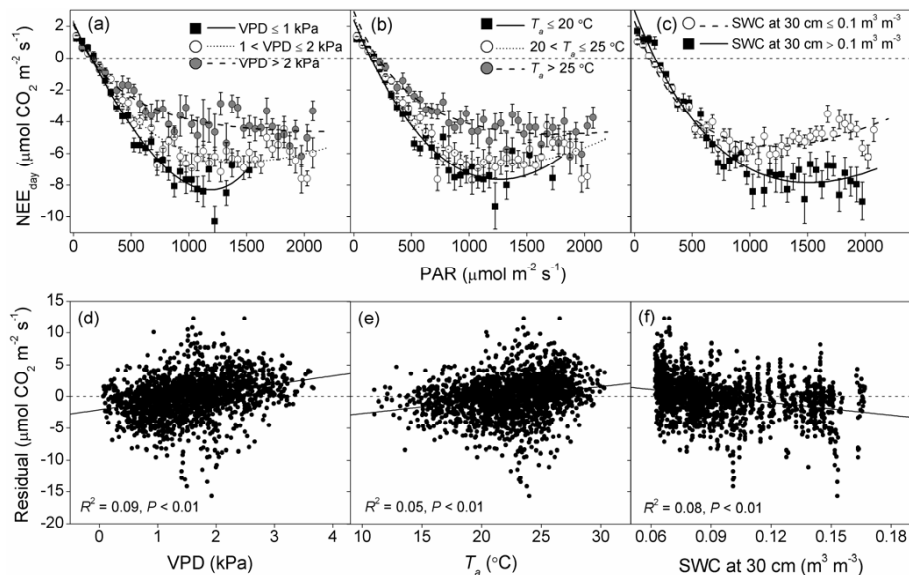
Fig. 2. Daytime net ecosystem CO_2 exchange (NEE_{day}) as a function of incident photosynthetically active radiation (PAR) for each month from May to October in 2012. Half-hourly NEE_{day} was bin-averaged into $50\,\mu mol\,m^{-2}\,s^{-1}$ PAR increments. Bars indicate standard errors. Light response curves were fit with Eq. (1). The dashed lines represent $y = 0$.

Fig. 3. Daytime net ecosystem CO_2 exchange (NEE_{day}) as a function of incident photosyntheti-cally active radiation (PAR) under different environmental conditions **(a–c)** and the relationships between residuals of the light response curve and environmental factors **(d–f)**. Only data from the peak growing season (June–August) were used to minimize the confounding effects of phenology. Half-hourly NEE_{day} was bin-averaged into $50\,\mu mol\,m^{-2}\,s^{-1}$ PAR increments in **(a–c)**. Bars indicate standard errors. Light response curves were fit with Eq. (1). The horizontal dashed lines represent $y = 0$.
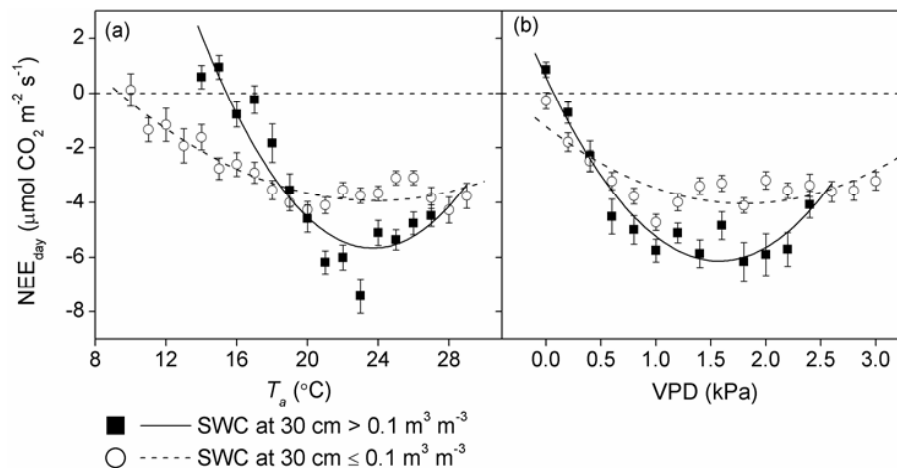
Fig. 4. Responses of daytime net ecosystem CO_2 exchange (NEE_{day}) to air temperature (T_a) **(a)** and vapor pressure deficit (VPD) **(b)** under different soil water contents (SWC) measured at 30 cm depth. Only data from the peak growing season (June–August) were used to minimize the confounding effects of phenology. Half-hourly NEE_{day} was bin-averaged into $1\,^\circ C\ T_s$ **(a)** and 0.2 kPa VPD **(b)** intervals, respectively. Bars indicate standard errors. Response curves were fit using the quadratic model. The horizontal dashed lines represent $y = 0$.

Title Page

Abstract   Introduction

Conclusions   References

Tables   Figures

Back   Close

Full Screen / Esc

Printer-friendly Version

Interactive Discussion
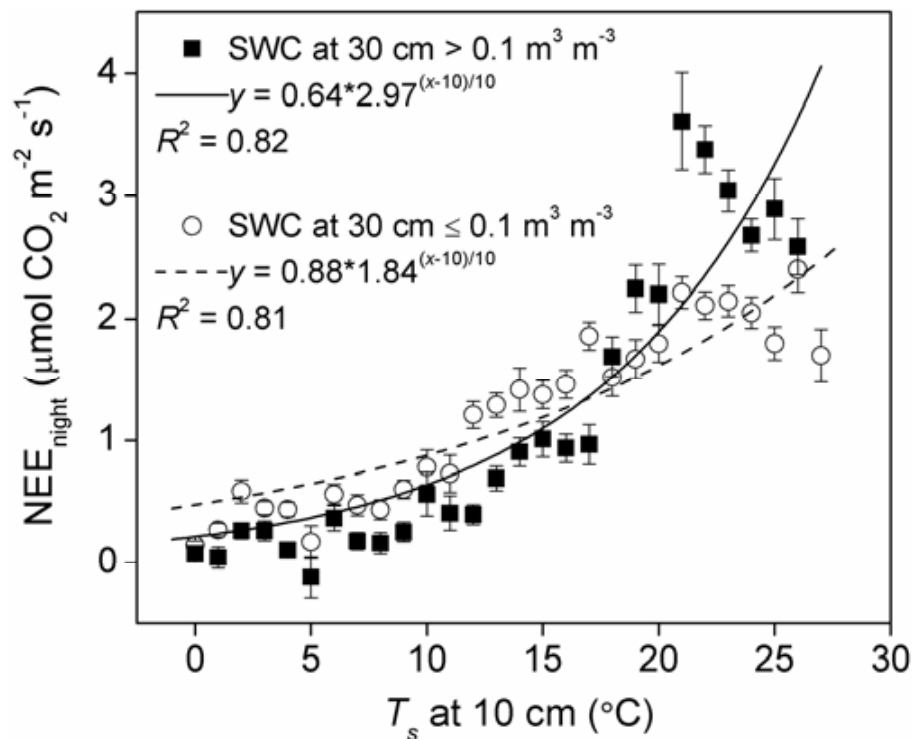
Fig. 5. Nighttime net ecosystem CO_2 exchange (NEE_{night}) as a function of soil temperature (T_s) at 10 cm depth under different soil water contents (SWC) measured at 30 cm depth. Only data when $T_s > 0\,°C$ were used. Half-hourly NEE_{night} was bin-averaged into $1\,°C$ T_s intervals. Error bars indicate standard errors.

Discussion Paper | Discussion Paper | Discussion Paper | Discussion Paper

BGD

11, 5089–5122, 2014

Biophysical controls on NEE over a semiarid shrubland

X. Jia et al.

Title Page

Abstract | Introduction

Conclusions | References

Tables | Figures

|◀ | ▶|

◀ | ▶

Back | Close

Full Screen / Esc

Printer-friendly Version

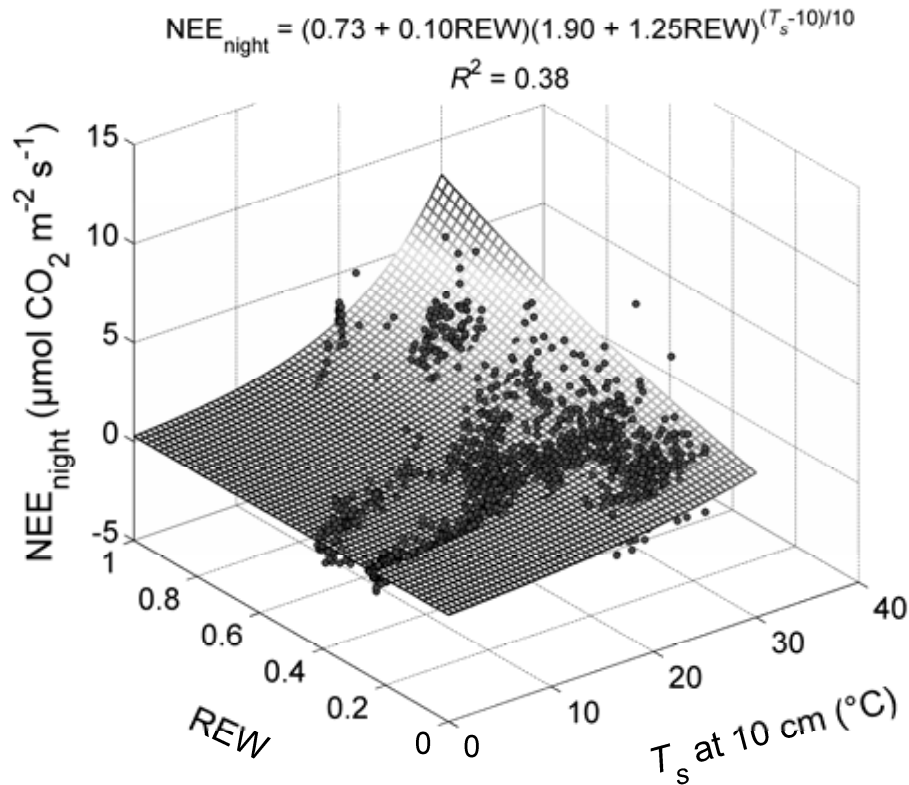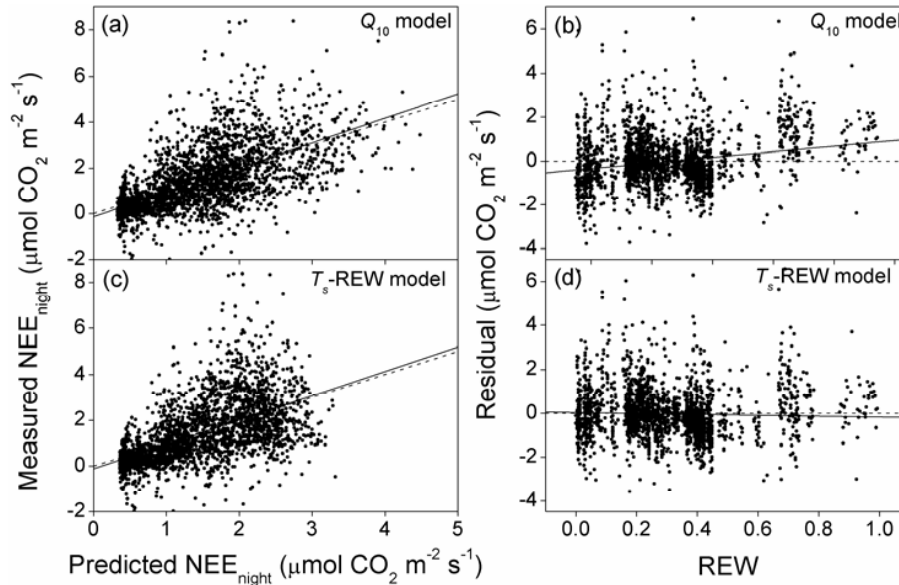Interactive Discussion

Fig. 6. Nighttime net ecosystem CO_2 exchange (NEE_{night}) as a function of soil temperature (T_s) at 10 cm depth and relative extractable water content (REW, see Eq. 10). Only data when $T_s > 0\,°C$ were used.

Fig. 7. Comparisons of measured and predicted half-hourly nighttime net ecosystem CO_2 exchange (NEE_{night}) using the Q_{10} model **(a)** and the T_s-REW model **(c)**; relationships between NEE_{night} residuals and REW for the Q_{10} model **(b)** and the T_s-REW model **(d)**. REW means the relative extractable water content (see Eq. 10). Only data when $T_s > 0\,°C$ were used. The dashed-lines in **(a)** and **(c)** represent $y = x$, and those in **(b)** and **(d)** represent $y = 0$. The fit line in **(a)**: $y = 1.08x - 0.14$, $R^2 = 0.33$, $P < 0.01$; the fit line in **(c)**: $y = 1.06x - 0.11$, $R^2 = 0.39$, $P < 0.01$. The slope and intercept as well as their 95 % confidence intervals (CI) are 1.27 (1.04, 1.50) and −0.40 (−0.48, −0.32) for the relationship between REW and the NEE_{night} residuals from the Q_{10} model **(b)**, and are −0.21 (−0.43, 0.02) and 0.03 (−0.05, 0.11) for the relationship between REW and the NEE_{night} residuals from the T_s-REW model **(d)**.
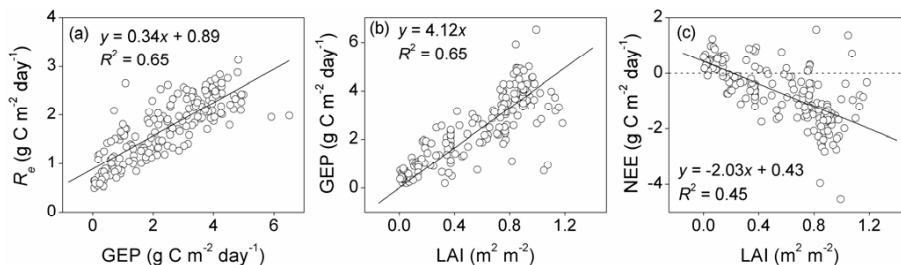
Fig. 8. Relationship between gross ecosystem productivity (GEP) and ecosystem respiration (R_e) **(a)**, and between leaf area index (LAI) and GEP **(b)** and net ecosystem CO_2 exchange (NEE) **(c)**. Daily values are shown for the growing period when LAI > 0. The horizontal dashed line in **(c)** represents $y = 0$.

Biophysical controls on NEE over a semiarid shrubland

X. Jia et al.

Title Page

Abstract | Introduction

Conclusions | References

Tables | Figures

|◄ | ►|

◄ | ►

Back | Close

Full Screen / Esc
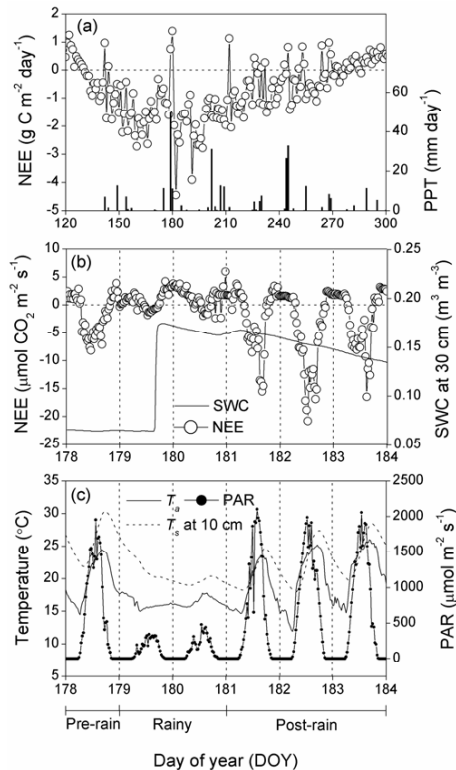
Printer-friendly Version

Interactive Discussion

Fig. 9. Pulses in daily net ecosystem CO_2 exchange (NEE) as related to precipitation (PPT) events during the growing season **(a)**, and synoptic variations of half-hourly NEE, soil water content (SWC) at 30 cm depth, air temperature (T_a), soil temperature at 10 cm depth (T_s) and incident photosynthetically active radiation (PAR) before and after a selected rainfall event **(b–c)**. The horizontal dashed lines in **(a)** and **(b)** represent $y = 0$, and the vertical dashed lines in **(b)** and **(c)** separate each day. PPT was 50 mm on DOY 179 and 11 mm on DOY 180.
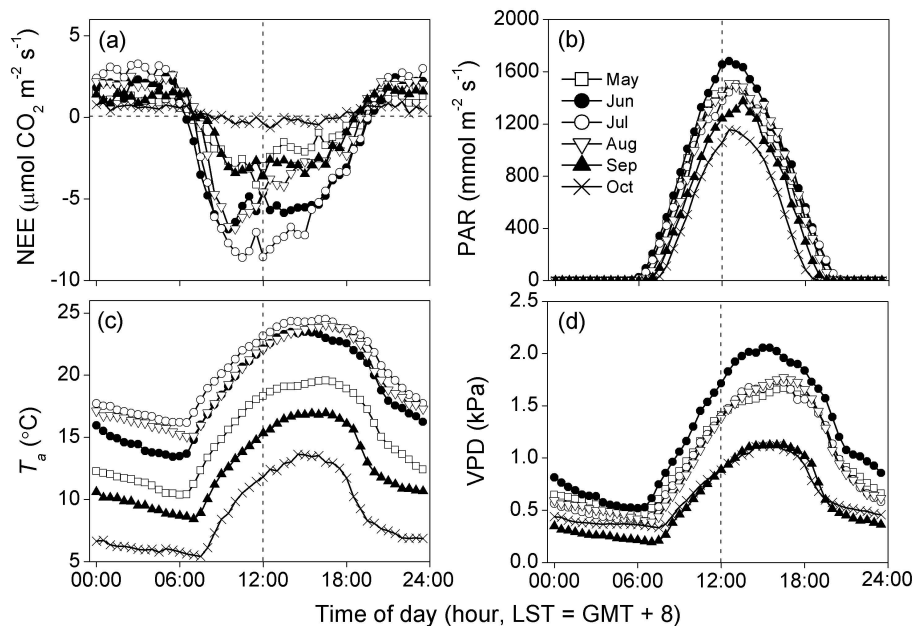
Fig. 10. Monthly mean diurnal cycles of net ecosystem CO_2 exchange (NEE) **(a)**, incident photosynthetically active radiation (PAR) **(b)**, air temperature (T_a) at 6 m aboveground **(c)** and vapor pressure deficit (VPD) **(d)**. The vertical dashed lines indicate noon, and the horizontal dashed line in **(a)** represents $y = 0$.

Title Page

Abstract | Introduction

Conclusions | References

Tables | Figures

|◄ | ►|

◄ | ►

Back | Close

Full Screen / Esc

Printer-friendly Version

Interactive Discussion